LUND UNIVERSITY

Electron localization following attosecond molecular photoionization

Sansone, G.; Kelkensberg, F.; Perez-Torres, J. F.; Morales, F.; Kling, M. F.; Siu, W.; Ghafur, O.; Johnsson, Per; Swoboda, Marko; Benedetti, E.; Ferrari, F.; Lepine, F.; Sanz-Vicario, J. L.; Zherebtsov, S.; Znakovskaya, I.; L'Huillier, Anne; Ivanov, M. Yu.; Nisoli, M.; Martin, F.; Vrakking, M. J. J.

Published in:
Nature

DOI:
10.1038/nature09084

2010

Link to publication

Citation for published version (APA):
Sansone, G., Kelkensberg, F., Perez-Torres, J. F., Morales, F., Kling, M. F., Siu, W., Ghafur, O., Johnsson, P., Swoboda, M., Benedetti, E., Ferrari, F., Lepine, F., Sanz-Vicario, J. L., Zherebtsov, S., Znakovskaya, I., L'Huillier, A., Ivanov, M. Y., Nisoli, M., Martin, F., & Vrakking, M. J. J. (2010). Electron localization following attosecond molecular photoionization. *Nature*, *465*(7299), 763-U3. https://doi.org/10.1038/nature09084

Total number of authors:
20

General rights
Unless other specific re-use rights are stated the following general rights apply:
Copyright and moral rights for the publications made accessible in the public portal are retained by the authors and/or other copyright owners and it is a condition of accessing publications that users recognise and abide by the legal requirements associated with these rights.
• Users may download and print one copy of any publication from the public portal for the purpose of private study or research.
• You may not further distribute the material or use it for any profit-making activity or commercial gain
• You may freely distribute the URL identifying the publication in the public portal

Read more about Creative commons licenses: https://creativecommons.org/licenses/

Take down policy
If you believe that this document breaches copyright please contact us providing details, and we will remove access to the work immediately and investigate your claim.

LUND UNIVERSITY

PO Box 117
221 00 Lund
+46 46-222 00 00

Download date: 16. Apr. 2024

Electron Localization following Attosecond Molecular Photoionization

G. Sansone[1*], F. Kelkensberg[2*], J. F. Pérez-Torres[3*], F Morales[3*], M.F. Kling[4], W. Siu[2], O.Ghafur[2], P. Johnsson[2,5], M. Swoboda[5], E. Benedetti[1], F. Ferrari[1], F. Lépine[6], J. L. Sanz-Vicario[7], S. Zherebtsov[4], I. Znakovskaya[4], A. L'Huillier[5], M. Yu. Ivanov[8], M. Nisoli[1], F. Martín[3], M.J.J. Vrakking[2,9]

[1]CNR-INFM, National Laboratory for Ultrafast and Ultraintense Optical Science, Department of Physics, Politecnico of Milan, Piazza L. da Vinci 32, 20133 Milano, Italy; [2]FOM-Institute AMOLF, Science Park 113, 1098 XG Amsterdam, The Netherlands; [3]Departamento de Química, C-9, Universidad Autónoma de Madrid, 28049 Madrid, Spain; [4]Max-Planck Institut für Quantenoptik, Hans-Kopfermann Strasse 1, D-85748 Garching, Germany; [5]Department of Physics, Lund University, PO Box 118, SE-221 00 Lund, Sweden ; [6]Université Lyon 1; CNRS; LASIM, UMR 5579, 43 bvd. Du 11 Novembre 1918, F-69622 Villeurbane, France ; [7]Grupo de Física Atómica y Molecular. Instituto de Física, Universidad de Antioquia, Medellín, Colombia; [8] National Research Council of Canada, Ottawa, Ontario K1A 0R6, Canada; [9]Max-Born-Institut, Max-Born Straße 2A, D-12489 Berlin, Germany

[*] *These people contributed equally to this work.*

The development of attosecond laser pulses allows one to probe the inner workings of atoms and molecules on the timescale of the electronic response [1-4]. In molecules, attosecond pump-probe spectroscopy enables investigations of the prompt charge redistribution and localization that accompany photo-excitation processes, where a molecule is lifted from the ground Born-Oppenheimer potential energy surface to one or more excited surfaces, and where subsequent photochemistry evolves on femtosecond timescales. Here we present the first example of a molecular

attosecond pump-probe experiment. H_2 and D_2 are dissociatively ionized by the sequence of an isolated attosecond pulse and an intense infrared few-cycle pulse. A localization of the electronic charge distribution within the molecule is measured that depends – with attosecond time-resolution – on the delay between the pump and probe pulses. The localization is shown to rely on two mechanisms. In mechanism I, it arises due to quantum mechanical interference between dissociation channels involving the $Q_1\ ^1\Sigma_u^+$ doubly-excited states and ionization continua where the infrared laser alters the angular momentum of the departing electron. In mechanism II, the charge localization arises during dissociation of the molecular ion and is due to laser-driven population transfer between the $1s\sigma_g$ and the $2p\sigma_u$ electronic states. These results open the way for attosecond pump-probe strategies to investigate the complex molecular dynamics that result from the coupling between electronic and nuclear motions beyond the usual Born-Oppenheimer approximation.

Following the successful development of isolated attosecond (1 as = 10^{-18} s) laser pulses less than a decade ago,[5] pioneering work on their use in studies of atomic photo-excitation and –ionization,[6,7] and in studies of electron dynamics in solids,[8] has raised the prospects that the molecular sciences may similarly benefit from the introduction of attosecond techniques. While the timescale for chemical re-arrangements that involve elaborate motion of the constituent atoms is necessarily in the femtosecond (1 fs = 10^{-15} s) domain, the electronic re-arrangement that accompanies the sudden removal or excitation of a selected electron is intrinsically faster. Indeed the removal of electrons that are involved in chemical binding may result in hole dynamics on sub- or few-fs timescales in a wide range of systems including bio-molecules and bio-molecular complexes.[9,10] Extremely fast molecular dynamics involving electron correlation can

also be initiated by the excitation of doubly-excited states and by subsequent auto-ionization processes.[11,12]

The application of attosecond laser pulses to molecular (auto)-ionization and electron localization requires suitable experimental diagnostics. Existing experimental implementations of attosecond techniques [13-16] do not readily lend themselves towards intra-molecular electronic re-arrangement processes. Here we introduce the measurement of angular asymmetries in the momentum distributions of fragments that result from dissociative ionization as a tool that is directly related to charge dynamics. As a benchmark, we investigate the dissociative ionization of hydrogen molecules (H_2, D_2). In the following we will mainly present experimental results for the case of D_2, where the highest quality data was acquired. Likewise, we present computational results for the case of H_2, where the close-coupling calculations presented below allow a more extensive exploration of the experimental conditions. To validate these calculations we will occasionally compare with H_2 measurements, whose quality is lower but which show analogous behavior to the D_2 measurements.

The choice of the hydrogen molecule as the subject of our investigation follows a rich tradition.[17,18] An attractive feature of H_2 is that its (intense field) dissociative ionization can frequently be understood in terms of the two lowest electronic states of the molecular ion, namely the $^2\Sigma_g^+(1s\sigma_g)$ and $^2\Sigma_u^+(2p\sigma_u)$ states (see Figure 1a). In our experiment (see Methods), the combination of an isolated attosecond XUV pulse[19] with a spectrum that extended from 20 to 40 eV and a (time-delayed) intense 6 fs FWHM IR pulse, with identical linear polarization, produced ionic fragments H^+ and D^+. The velocity and angular distribution were measured.[20] In D^+ ion kinetic energy spectra recorded without the IR beam (Figure 1b), a broad kinetic energy distribution is observed, consistent with earlier experimental and theoretical work.[21] To interpret these (see Figure 1c) and all later results, we have solved the time-dependent Schrödinger

equation (TDSE) for H_2 by using a close-coupling method that includes the bound states, the $^2\Sigma_g^+(1s\sigma_g)$ and the $^2\Sigma_u^+(2p\sigma_u)$ ionization continua, and the doubly excited states embedded in them.[12] The calculations take into account all electronic and vibrational (dissociative) degrees of freedom, and include the effect of electron correlation and interferences between different ionization and dissociation pathways (see Methods). From here on, we will focus on the detection of fragments from molecules that are aligned parallel to the laser polarization axis. Therefore in the calculations only states of Σ symmetry were included.

Upon XUV excitation, several pathways lead to dissociative ionization. The relative weights depend on the photon energy and the observation angle of the ionic fragment with respect to the laser polarization.[21] Up to hν = 25 eV, direct ionization forms the $^2\Sigma_g^+(1s\sigma_g)$ state , and releases a small fraction (2%) of low kinetic energy (E_k < 1 eV) ionic fragments. Between hν = 25 eV and hν = 36 eV, a parallel transition preferentially excites molecules aligned along the polarization axis to the doubly-excited Q_1 $^1\Sigma_u^+$ states. Subsequent auto-ionization to the $^2\Sigma_g^+(1s\sigma_g)$ state produces fragments with a kinetic energy that spans the entire range of 0-10 eV, but lies primarily between 2 and 7 eV.[22, 23] Direct ionization to the repulsive $^2\Sigma_u^+(2p\sigma_u)$ state becomes possible at hν = 30 eV. Above hν = 38 eV the full range of internuclear distances sampled by the ground state of H_2 can participate in this channel, leading to high-energy fragments (E_k = 5 - 10 eV). Above 31 eV, a perpendicular transition preferentially excites molecules that are orthogonally aligned to the laser polarization axis to the Q_2 $^1\Pi_u$ doubly-excited states. These states auto-ionize to both the $^2\Sigma_g^+(1s\sigma_g)$ and the $^2\Sigma_u^+(2p\sigma_u)$ states, resulting in ionic fragments with kinetic energies of 1-5 eV and 5-8 eV, respectively.[21] Since the evaluation of the kinetic energy distributions in the experiment forces us to include ionic fragments within a 45 degree cone around the laser polarization axis, involvement of the Q_2 $^1\Pi_u$ states cannot *a priori* be ruled out.

When the molecule furthermore interacts with a few-cycle IR pulse, a number of changes occur in the fragment kinetic energy distributions. Experimental D^+ and calculated H^+ kinetic energy distributions are shown as a function of the relative delay τ between the attosecond and IR pulses in Fig. 1d and 1e. Note that in view of the very demanding nature of the computations, calculations could be performed for IR intensities up to $3 \cdot 10^{12}$ W/cm^2 and for XUV-IR delays of up to 12 fs. Experimentally we estimate the IR intensity may have been higher by as much as a factor of 2.

At low energy (E_k < 1 eV) bond-softening of the bound $^2\Sigma_g^+(1s\sigma_g)$ vibrational wave packet by the IR pulse is observed. The bond-softening peaks at τ = +10 fs, when the wave packet finds itself near the outer turning point of the potential energy curve.[24,25] When the XUV and IR pulses overlap ($\tau \approx 0$ fs), a strong increase of the ion signal at high energy (around 8 eV) is observed, accompanied by a decrease at intermediate energies (3 eV < E_k < 5 eV). Based on the close-coupling calculations, we believe this enhancement is due to an increase of the excitation cross-section of the $2p\sigma_u$ continuum due to IR-laser induced mixing of the $2p\sigma_u$ and $1s\sigma_g$ states. The increase may furthermore contain contributions from photo-ionization of the Q_1 $^1\Sigma_u^+$ doubly-excited states by the IR laser. For larger time delays (τ > 8 fs), the kinetic energy distribution above 1 eV does not change appreciably with delay and resembles the distribution obtained in the absence of the IR field (see Fig. 1b and 1c).

Dissociative ionization of H_2 lends itself to the observation of both laboratory-frame and molecular-frame asymmetries. The former corresponds to an asymmetry in the fragment ejection along the laser polarization axis, while the latter corresponds to a (anti-)correlation in the direction of emission of the ionized electron and the ionic fragment. Laboratory-frame asymmetries were previously observed in dissociative ionization of D_2 by a carrier-envelope phase (CEP)-locked infrared laser pulse,[26] while

symmetry-breaking in the molecular frame was observed in single-photon XUV dissociative ionization of H_2 and D_2, mediated by auto-ionization of the $Q_2\ ^1\Pi_u$ state.[27]

In the present experiment laboratory-frame asymmetries $A(E_k, \tau)$ were defined as

$$A(E_k, \tau) = \{N_L(E_k, \tau) - N_R(E_k,\tau)\}/\{N_L(E_k, \tau) + N_R(E_k,\tau) + \delta\} \quad (1)$$

where $N_{L,R}(E_k,\tau)$ indicates the number of ions arriving within 45 degrees from the polarization axis on the left and right side of the detector and δ is a small number that prevents a singularity when $N_L(E_k, \tau) + N_R(E_k,\tau)$ vanishes.

Over almost the entire kinetic energy range where D^+ resp. H^+ ions are formed, asymmetries are observed that oscillate as a function of τ, as shown in Figure 2a and 2c. Delaying the IR laser by one-quarter of the IR period (650 as) or by one-half of the IR period (1.3 fs) leads to a disappearance or reversal of the electron localization. The phase of the asymmetry oscillations strongly depends on the kinetic energy of the fragment that is measured.

The asymmetries can be understood by writing the two-electron wave function of singly-ionized H_2 as:

$$\Psi = c_1[1s\sigma_g(1)\ \varepsilon l_g(2)]_g + c_2[1s\sigma_g(1)\ \varepsilon l_u(2)]_u + c_3[2p\sigma_u(1)\ \varepsilon l_u(2)]_g + c_4[2p\sigma_u(1)\ \varepsilon l_g(2)]_u \quad (2)$$

where, for simplicity, the wave function has not been anti-symmetrized with respect to electrons 1 and 2, and the ionized electron 2 is described by a continuum orbital of well defined energy ε and angular momentum l_g or l_u. The observation of a fragment asymmetry relies on the formation of a mixed-parity superposition state that contains contributions (at the same fragment kinetic energy and for the same angular momentum l_u or l_g) from both the $1s\sigma_g$ and the $2p\sigma_u$ states. This can be recognized from the

following expressions for wave-functions of $H_2^+ + e^-$ that have the bound electron localized on the left or right proton:

$$\Psi_L = [1s\sigma_g(1) + 2p\sigma_u(1)]\, \varepsilon l_{g,u}(2)$$

$$\Psi_R = [1s\sigma_g(1) - 2p\sigma_u(1)]\, \varepsilon l_{g,u}(2) \qquad (3)$$

From equations (1-3), it is very easy to see that

$$N_L(E_k,t) - N_R(E_k,t) = 4\ \mathrm{Re}\,[c_1 c_4^* + c_2 c_3^*]$$

Thus a laboratory frame asymmetry is formed by a mixed-parity superposition where the continuum electron has the same angular momentum $l_{u/g}$ in both ionic states, (c_1,$c_4 \neq 0$) resp. (c_2,$c_3 \neq 0$).[26] In contrast, a molecular frame asymmetry is caused by an interference of the first (second) and the third (fourth) term in equation (2) (c_1,$c_3 \neq 0$ or c_2,$c_4 \neq 0$).[27]

$A(E_{k,}\tau)$ can be accurately evaluated from the two-electron wave function obtained in the close-coupling calculation. As can be seen in Figure 2b, the close coupling calculations reproduce the occurrence of oscillations in $A(E_{k,}\tau)$ with the periodicity of the IR laser. The asymmetry oscillations are very pronounced for delays up to 7 fs and kinetic energies above 5 eV and decrease in amplitude for delays beyond 7 fs and kinetic energies below 5 eV.

In the absence of the IR, the XUV photo-ionization produces a two-electron wave function where only c_2 and c_4 are non-zero, thereby precluding the observation of a laboratory-frame asymmetry. The IR laser can cause an asymmetry either by changing the wave function of the continuum electron or by changing the wave function of the molecular ion. The former occurs as a result of the influence of the IR laser during the photo-excitation process (this will henceforth be called: mechanism I, Fig. 3a), while

the latter occurs as a result of the interaction of the molecular ion with the IR laser during the dissociation process (this will henceforth be called: mechanism II, Fig. 3c).

The asymmetry oscillations in Figure 2b in the region where the XUV and IR pulses overlap ($\tau < 8$ fs) occur under conditions where XUV-only ionization produces high-energy fragments (from excitation of the $2p\sigma_u$ state) accompanied by the emission of an s-electron ($c_4 \neq 0$). However, the interaction of the IR laser with this photoelectron redistributes the wave function over several angular momentum states, including the p-continuum ($c_3 \neq 0$, see figure in supplementary information). At the same time, auto-ionization of the $Q_1\ ^1\Sigma_u^+(1)$ state (and, to a lesser extent, direct ionization) leads to the formation of a dissociative wave packet on the $1s\sigma_g$ state that is primarily accompanied by the emission of a *p*-electron ($c_2 \neq 0$, see figure in supplementary information). Further support for the involvement of the $Q_1\ ^1\Sigma_u^+(1)$ state is suggested by results of a close-coupling calculation in which direct excitation to the $1s\sigma_g$ state by the XUV pump was artificially suppressed (see Fig. 3b): fringes in the region $\tau < 7$ fs and $E_k > 5$ eV are then still apparent, even though no wave packet is initially produced in the $1s\sigma_g$ state. To summarize, our mechanism I (Fig. 3a) explains the asymmetry oscillations that are observed for temporal overlap of the XUV and IR pulses in terms of the interference of a wave packet on the $1s\sigma_g$ state that is mainly formed by auto-ionization of the $Q_1\ ^1\Sigma_u^+(1)$ doubly-excited state with a wave packet on the $2p\sigma_u$ state that is formed by an XUV photo-ionization process where the continuum electron absorbs one or more photons from the IR field.

Mechanism I can only occur when the XUV and IR pulses overlap. In contrast, mechanism II requires that the IR has a high intensity during the dissociation of the molecule, irrespective of whether the IR and XUV pulses themselves overlap. The IR-laser can induce population transfer between a wave packet dissociating on the $2p\sigma_u$ state and the $1s\sigma_g$ state (see Fig. 3c). Since the close coupling calculations were

restricted to intensities ≤ $3x10^{12}$ W/cm^2 and to the excitation of Σ-states, this mechanism is only weakly visible in Fig 2b. Nevertheless this mechanism is expected to be dominant at the intensities where the experiments were performed and clearly shows up in calculations performed by numerical integration of the 1D TDSE that describe the evolution of a vibrational wave packet initially placed in the $2p\sigma_u$ state of the H_2^+ (see Fig. 3d). Moreover, under our experimental conditions the potential involvement of the Q_2 $^1\Pi_u$ doubly excited states implies a larger population of the $2p\sigma_u$ states than in the calculations and, therefore, a reinforcement of the asymmetry at long delays in the region $E_k > 5$ eV.

Similar results as in figure 3d are obtained by an even simpler semi-classical Landau-Zener (LZ) model (see Methods). In this model the IR-laser induced population transfer during dissociation can be understood in terms of so-called quasi-static states, which are the eigenstates of the $1s\sigma_g/2p\sigma_u$ two-level problem in the presence of a (static) electric field:

$$\Psi_1 = \cos\theta(t)\,(1s\sigma_g) + \sin\theta(t)\,(2p\sigma_u)$$

$$\Psi_2 = -\sin\theta(t)\,(1s\sigma_g) + \cos\theta(t)\,(2p\sigma_u) \qquad (4)$$

where $\theta(t)$ is related to the splitting $\omega_0(R)$ between the $1s\sigma_g$ and $2p\sigma_u$ states and to the IR laser-induced dipole coupling $V_{g,u}(R,t) = -\mu(R)E(t)$ by[28]

$$\tan 2\theta(t) = -2V_{g,u}(R,t)/\omega_0(R) \qquad (5)$$

Early on, when $\omega_0(R) >> \mu(R)E_0(t)$, the Landau-Zener transition probability is small and the nuclear wave packet remains in Ψ_2. When $\omega_0(R) \approx \mu(R)E_0(t)$, the nuclear wave packet breaks up into a coherent superposition of the quasi-static states, which now furthermore begin to resemble the localized states Ψ_L and Ψ_R. Towards the end of the dissociation, $\omega_0(R) << \mu(R)E_0(t)$, the nuclear wave packet switches between the two

quasi-static states. This merely reflects the fact that the electron is no longer able to switch from left to right and ensures that the localization acquired in the intermediate region persists. The correlated dependence of the asymmetry on E_k and τ is caused by the dependence of the localization process on the internuclear distance where the nuclear wave packet is launched.

Rapid electronic processes on timescales extending down into the attosecond domain define our natural environment, and are at the heart of photo-physical, photo-chemical and photo-biological processes that sustain and enable life. In this work the first comprehensive experimental and computational effort has been presented aiming at and demonstrating the utility of attosecond pulses in molecular science thereby establishing a point of departure for the direct investigation of (multi)-electron dynamics in molecular systems, such as electron transfer/localization and auto-ionization, and of the coupling between electronic and nuclear degrees of freedom on timescales approaching the atomic unit of time.

Methods summary

Experimental methods. To generate both beams, linearly polarized few-cycle IR laser pulses with a controlled CEP were divided into a central and annular part using a drilled mirror. The polarization state of the central part was modulated in time using two birefringent plates in order to obtain a short temporal window of linear polarization around the center of the pulse. This laser beam was focused in a Krypton gas jet to generate an XUV continuum via high-order harmonic generation.[29] A 100 nm aluminum filter was used to eliminate low-order harmonics and the IR radiation, and provided a partial dispersion compensation of the transmitted XUV light. In this way single attosecond pulse with a duration between 300-400 as were produced.[19] The attosecond pulses were focused using a grazing incidence toroidal mirror into the interaction region

of a Velocity Map Imaging Spectrometer (VMIS). The annular part of the original IR beam was focused by a spherical mirror and collinearly recombined with the attosecond pulse using a second drilled mirror. The relative time delay between the two pulses was changed with attosecond time resolution using a piezoelectric stage inserted in the interferometric setup. The XUV and IR laser beams were crossed with an effusive H_2/D_2 gas jet that emerged from a 50 μm diameter capillary that was incorporated into the repeller electrode of the VMIS.[30] Ions generated in the two-color dissociative ionization were projected onto an MCP + phosphor screen detector. 2D ion images were acquired using a low-noise CCD camera, and allowed retrieval of the 3D velocity distribution of the ions.

Methods

Experimental methods. To generate both beams, linearly polarized few-cycle IR laser pulses with a controlled CEP were divided into a central and annular part using a drilled mirror. The polarization state of the central part was modulated in time using two birefringent plates in order to obtain a short temporal window of linear polarization around the center of the pulse. This laser beam was focused in a Krypton gas jet to generate an XUV continuum via high-order harmonic generation.[29] A 100 nm aluminum filter was used to eliminate low-order harmonics and the IR radiation, and provided a partial dispersion compensation of the transmitted XUV light. In this way single attosecond pulses with a duration between 300-400 as were produced.[18] The attosecond pulses were focused using a grazing incidence toroidal mirror into the interaction region of a Velocity Map Imaging Spectrometer (VMIS). The annular part of the original IR beam was focused by a spherical mirror and collinearly recombined with the attosecond pulse using a second drilled mirror. The relative time delay between the two pulses was changed with attosecond time resolution using a piezoelectric stage inserted in the interferometric setup. The XUV and IR laser beams were crossed with an effusive

H_2/D_2 gas jet that emerged from a 50 μm diameter capillary that was incorporated into the repeller electrode of the VMIS.[30] Ions generated in the two-color dissociative ionization were projected onto an MCP + phosphor screen detector. 2D ion images were acquired using a low-noise CCD camera, and allowed retrieval of the 3D velocity distribution of the ions.

Numerical methods. The two-electron close-coupling calculations have been performed by using an extension of the method reported in Ref. [12]. Briefly, we have solved the seven dimensional (7D) time-dependent Schrödinger equation

$$\left(\hat{H}^0(\mathbf{r}_1,\mathbf{r}_2,R)+V(t)-i\frac{\partial}{\partial t}\right)\Phi(\mathbf{r}_1,\mathbf{r}_2,R,t)=0$$

where $\mathbf{r}_1$, $\mathbf{r}_2$ are the position vectors of electrons 1 and 2, respectively (two times 3D), R is the internuclear distance (1D), $\hat{H}^0$ is the H_2 field-free non relativistic Hamiltonian, Φ is the time-dependent wave function, and $V(t)$ is the laser-H_2 interaction potential in the dipole approximation which is a sum of two terms corresponding to the XUV and IR pulses separated by a peak-peak time delay τ, $V(t) = V_{XUV}(t) + V_{IR}(t+\tau)$, , with frequencies ω_{XUV} and ω_{IR}, and durations T_{XUV} and T_{IR}, respectively. Each pulse has a cosine square temporal envelope and is given by the analytical formula

$$V_k(t') = \begin{cases} \mathbf{p}\cdot\mathbf{A}_k^0 \cos^2\left(\dfrac{\pi t'}{T_k}\right) & for\ -\dfrac{T_k}{2} \le t' \le \dfrac{T_k}{2} \\ 0 & elsewhere \end{cases}$$

where $t'=t$ for the XUV pulse, $t'=t+\tau$ for the IR pulse, and **p** is the dipole moment. In all calculations we have used ω_{XUV} = 30 eV, T_{XUV} = 400 as, $I_{XUV} = \left(A_{XUV}^0\right)^2 \omega_{XUV}^2 = 10^9$ W/cm^2, ω_{IR} = 1.65 eV, T_{IR} = 16 fs (corresponding to a pulse duration of 6 fs FWHM), $I_{XUV} = \left(A_{XUV}^0\right)^2 \omega_{XUV}^2 = 3\cdot10^{12}$ W/cm^2, and τ has been varied from 0 up to 12 fs. The TDSE has been solved by expanding the time-dependent wave function Φ in a basis of fully correlated H_2 vibronic stationary states of Σ_g^+ and Σ_u^+ symmetries, which include

the bound states, the non-resonant continuum states associated with the $1s\sigma_g$ and $2p\sigma_u$ ionization channels, and the lowest Q_1 and Q_2 doubly excited states. In doing so, the TDSE is effectively 6D and the results are exclusively valid for H_2 molecules oriented parallel to the polarization direction. The electronic part of the vibronic states is calculated in a box of 160 a.u. and the nuclear part in a box of 12 a.u.. The size of these boxes is large enough to ensure that there are no significant reflections of electronic and nuclear wave packets in the box boundaries for propagation times smaller than $\tau + (T_{XUV} + T_{IR})/2$. Non-adiabatic couplings and molecular rotations have been neglected.

The two-electron wave function that is obtained in the close-coupling calculation lends itself to a detailed analysis of the mechanisms that lead to the measurement of laboratory-frame asymmetries in the dissociative ionization of the molecule. As an example, the figure in the Supporting Information shows the angular momentum and electronic state-resolved delay dependence of H^+ ions with a fragment kinetic energy in the interval <7.5 eV, 8.5 eV>. Angular momentum l_g and l_u stand for $l_g = (1s\sigma_g \varepsilon l)_g$ and $l_u = (2p\sigma_u \varepsilon l)_u$ for $l = 0$ ($s_{g,u}$-wave), $l = 2$ ($d_{g,u}$-wave),…. and $l_g = (2p\sigma_u \varepsilon l)_g$ and $l_u = (1s\sigma_g \varepsilon l)_g$ for $l = 1$ ($p_{g,u}$-wave), $l = 3$ ($f_{g,u}$-wave),…. A (time-dependent) asymmetry is expected when for a given angular momentum a substantial population is simultaneously present in both the $1s\sigma_g$ and the $2p\sigma_u$ states (g and u).

In analyzing mechanism II, we have performed 1D TDSE calculations that describe the evolution of a wave packet initially located in the $2p\sigma_u$ state and centred at the H_2 equilibrium distance. In these calculations, only the $1s\sigma_g$ and $2p\sigma_u$ state were included and the IR pulse was launched at different times to simulate the delay τ between the pump and the probe pulses. We have also used the Landau-Zener model in which the transition probability between the two-dressed states of eq. (4) is given by [25]

$$W = \exp\left(\frac{-\pi\omega_0^2(R)}{4\omega_{IR}\mu(R)E_0(t)} \right)$$

where ω_{IR} is the carrier frequency of the laser and where $E_0(t)$ is the envelope of the laser pulse. This has been used to evaluate the probability for a diabatic transition and, hence, the population in the quasi-static states. This leads to an asymmetry parameter that is similar to that obtained from the 1D TDSE calculations.

1. Corkum, P. B. & Krausz, F. Attosecond science. *Nature Physics* **3**, 381-387 (2007).

2. Kapteyn, H., Cohen, O., Christov, I. & Murnane, M. Harnessing Attosecond Science in the Quest for Coherent X-rays. *Science* **317**, 775-778 (2007).

3. Kling, M. F. & Vrakking, M. J. J. Attosecond Electron Dynamics. *Annu. Rev. Phys. Chem.* **59**, 463-492 (2008).

4. Krausz, F. & Ivanov, M. Attosecond physics. *Rev. Mod. Phys.* **81**, 163-234 (2009).

5. Hentschel, M. et al. Attosecond metrology. *Nature* **414**, 509-513 (2001).

6. Drescher, M. et al. Time-resolved atomic inner-shell spectroscopy. *Nature* **419**, 803-807 (2002).

7. Uiberacker, M. et al. Attosecond real-time observation of electron tunnelling in atoms. *Nature* **446**, 627-632 (2007).

8. Cavalieri, A. L. et al. Attosecond spectroscopy in condensed matter. *Nature* **449**, 1029-1032 (2007).

9. Remacle, F. & Levine, R. D. An electronic time scale in chemistry. *PNAS* **103**, 6793-6798 (2006).

10. Kuleff, A.I. & Cederbaum, L.S. Charge migration in different conformers of glycine: The role of nuclear geometry. *Chem. Phys.* **338**, 320-328 (2007).

11. Wickenhauser, M., Burgdorfer, J., Krausz, F. & Drescher, M. Time Resolved Fano Resonances. *Phys. Rev. Lett.* **94**, 023002 (2005).

12. Sanz-Vicario, J. L., Bachau, H. & Martin, F. Time-dependent theoretical description of molecular autoionization produced by femtosecond xuv laser pulses. *Phys. Rev. A* **73**, 033410 (2006).

13. Kienberger, R. et al. Atomic transient recorder. *Nature* **427**, 817-821 (2004).

14. Uphues, T. et al. Ion-charge-state chronoscopy of cascaded atomic Auger decay. *New J. Phys.* **10**, 025009 (2008).

15. Remetter, T. et al. Attosecond electron wave packet interferometry. *Nature Physics* **2**, 323-326 (2006).

16. Mauritsson, J. et al. Attosecond Pump-Probe Electron Interferometry. (2009 (submitted for publication)).

17. Bucksbaum, P. H., Zavriyev, A., Muller, H. G. & Schumacher, D. W. Softening of the H_2^+ molecular bond in Intense Laser Fields. *Phys. Rev. Lett.* **64**, 1883-1886 (1990).

18. Frasinski, L. J. et al. Manipulation of Bond Hardening in H_2^+ by Chirping of Intense Femtosecond Laser Pulses. *Phys. Rev. Lett.* **83**, 3625-3628 (1999).

19. Sansone, G. et al. Isolated Single-Cycle Attosecond Pulses. *Science* **314**, 443-446 (2006).

20. Eppink, A. T. J. B. & Parker, D. H. Velocity map imaging of ions and electrons using electrostatic lenses: Application in photoelectron and photofragment ion imaging of molecular oxygen. *Rev. Sci. Instrum.* **68**, 3477-3484 (1997).

21. Ito, K., Hall, R. I. & Ukai, M. Dissociative photoionization of H_2 and D_2 in the energy region of 25-45 eV. *J. Chem. Phys.* **104**, 8449-8457 (1996).

22. Sanchez, I. & Martin, F. Origin of Unidentified Structures in Resonant Dissociative Photoionization of H_2. *Phys. Rev. Lett.* **79**, 1654-1657 (1997).

23. Sanchez, I. & Martin, F. Resonant dissociative photoionization of H_2 and D_2. *Phys. Rev. A* **57**, 1006-1017 (1998).

24. Rudenko, A. et al. Real-time observation of vibrational revival in the fastest molecular system. *Chem. Phys.* **329**, 193-202 (2006).

25. Kelkensberg, F. et al. Molecular Dissociative Ionization and Wave-Packet Dynamics studied using Two-Color XUV and IR Pump-Probe Spectroscopy. *Phys. Rev. Lett. 103, 123005 (2009).*

26. Kling, M. F. et al. Control of Electron Localization in Molecular Dissociation. *Science* **312**, 246-248 (2006).

27. Martin, F. et al. Single Photon-Induced Symmetry Breaking of H_2 Dissociation. *Science* **315**, 629-633 (2007).

28. Dietrich, P., Ivanov, M. Y., Ilkov, F. A. & Corkum, P. B. Two-Electron Dissociative Ionization of H_2 and D_2 in Infrared Laser Fields. *Phys. Rev. Lett.* **77**, 4150-4153 (1996).

29. Sola, I. J. et al. Controlling attosecond electron dynamics by phase-stabilized polarization gating. *Nature Physics* **2**, 319-322 (2006).

30. Ghafur, O., Siu, W., Kling, M., Drescher, M. & Vrakking, M. J. J. A velocity map imaging detector with an integrated gas injection system. *Rev. Sci. Instrum.* **80** (2009).

Supplementary Information is linked to the online version of the paper at www.nature.com/nature.

Acknowledgements This work is part of the research programs of the "Stichting voor Fundamenteel Onderzoek der Materie (FOM)", which is financially supported by the "Nederlandse organisatie voor Wetenschappelijk Onderzoek (NWO)", and of the Spanish Ministerio de Ciencia e Innovación, project no. FIS2007-60064 . Support by MC-RTN "XTRA" (FP6-505138), the MC-EST MAXLAS, Laserlab Europe (Integrated Infrastructure Initiative Contract RII3-CT-2003-506350, proposal cusbo001275), the European COST Action "CUSPFEL" (CM0702), the Mare Nostrum Barcelona Supercomputer Center (BSC), the Centro de Computación Científica UAM, the Netherlands National Computing Facilities foundation (NCF), Stichting Academisch Rekencentrum Amsterdam (SARA), the Alban Program for Latin-America (E07D401391CO), the Universidad de Antioquia, the COLCIENCIAS agency, the Swedish Research Council, the DFG via the Emmy-Noether program and the Cluster of Excellence: Munich Center of Advanced Photonics.

Author Contributions G.S., F.K., J.F.P.T. and F.M. contributed equally to this work. G.S. was responsible for the construction of the attosecond pump-probe set-up and the experiments on H_2 and D_2. F.K. was responsible for the experiments on H_2 and D_2 and the development of the semi-classical model. J.F.P.T. and F.M. were responsible for the construction of the close-coupling code and the calculations using this code.

Author Information Correspondence and requests for materials should be addressed to M.V. (m.vrakking@amolf.nl).

Figure 1: Dissociative ionization of hydrogen by an XUV-IR pulse sequence (a) Photo-excitation of neutral hydrogen leads to the excitation of the Q_1 (red) and Q_2 (blue) doubly-excited states and ionization to the $1s\sigma_g$ and $2p\sigma_u$ states, which can be followed by dissociation.; (b) experimental D^+ and (c) calculated H^+ kinetic energy distributions with only the isolated attosecond laser pulse present, with only the few-cycle IR laser pulse present, and for two delays

between the XUV the IR pulse ; (d) experimental D^+ and (e) calculated H^+ kinetic energy distributions as a function of the delay between the attosecond pulse and the IR pulse.

Figure 2: Asymmetry in XUV+IR dissociative ionization of hydrogen (a) Experimentally measured asymmetry parameter for the formation of D^+-ions in two-color XUV+IR dissociative ionization of D_2, as a function of the fragment kinetic energy E_k and the XUV-IR delay. A fragment asymmetry is observed that oscillates as a function of the XUV-IR delay and that strongly depends on the kinetic energy.; (b) Calculated asymmetry parameter for the formation of H^+ ions in two-color XUV+IR dissociative ionization of H_2 as a function of the fragment kinetic energy E_k and the XUV-IR delay, obtained using the close-coupling method described in the text; (c) similar to (a) but for H^+-ions

Figure 3: Mechanisms that lead to asymmetry in XUV+IR dissociative ionization. (a) asymmetry caused by the interference of a wavepacket launched on the $2p\sigma_u$ state by direct XUV ionization or rapid ionization of the Q_1 $^1\Sigma_u^+$ states by the IR, and a wavepacket on the $1s\sigma_g^+$ state resulting from autoionization of the Q_1 $^1\Sigma_u^+$ states. Blue arrows signify the role of the XUV pulse, and red arrows that of the IR pulse; purple lines and arrows signify dynamics that is intrinsic to the molecule; (b) close-coupling calculations where direct photo-excitation to the $1s\sigma_g$ state has been excluded, supporting the notion that the Q_1 autoionizing states play an important role in the localization dynamics; (c) asymmetry caused by the interference of a wavepacket that is launched on the $2p\sigma_u$ state by direct XUV ionization and a wavepacket on the

$1s\sigma_g$ state that results from stimulated emission during the dissociation process; (d) time-dependent asymmetry calculated by a two-level calculation where the wave function of the dissociating molecule is considered as a coherent superposition of the $1s\sigma_g$ and $2p\sigma_u$ states.

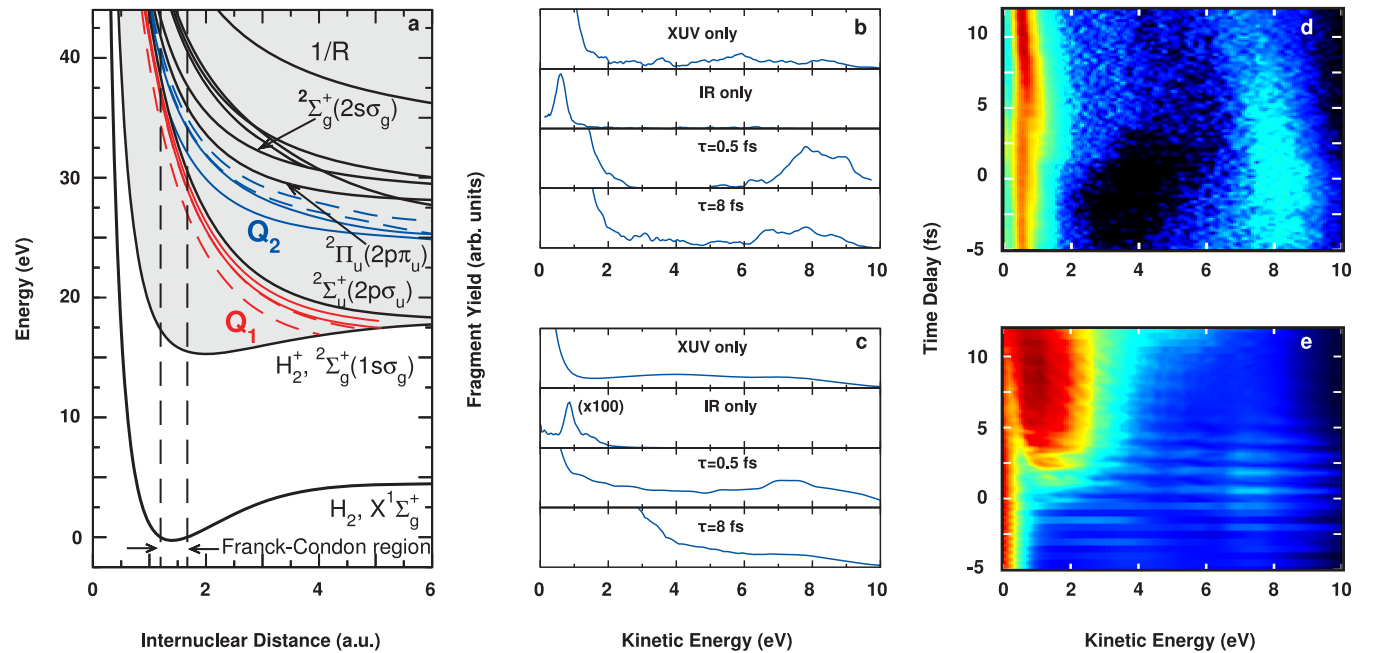
a
1/R
$^2\Sigma_g^+(2s\sigma_g)$
Q_2
$^2\Pi_u(2p\pi_u)$
$^2\Sigma_u^+(2p\sigma_u)$
Q_1
H_2^+, $^2\Sigma_g^+(1s\sigma_g)$
H_2, $X^1\Sigma_g^+$
Franck-Condon region
Energy (eV)
Internuclear Distance (a.u.)
b
XUV only
IR only
τ=0.5 fs
τ=8 fs
c
XUV only
(x100)
IR only
τ=0.5 fs
τ=8 fs
Fragment Yield (arb. units)
Kinetic Energy (eV)
d
e
Time Delay (fs)
Kinetic Energy (eV)

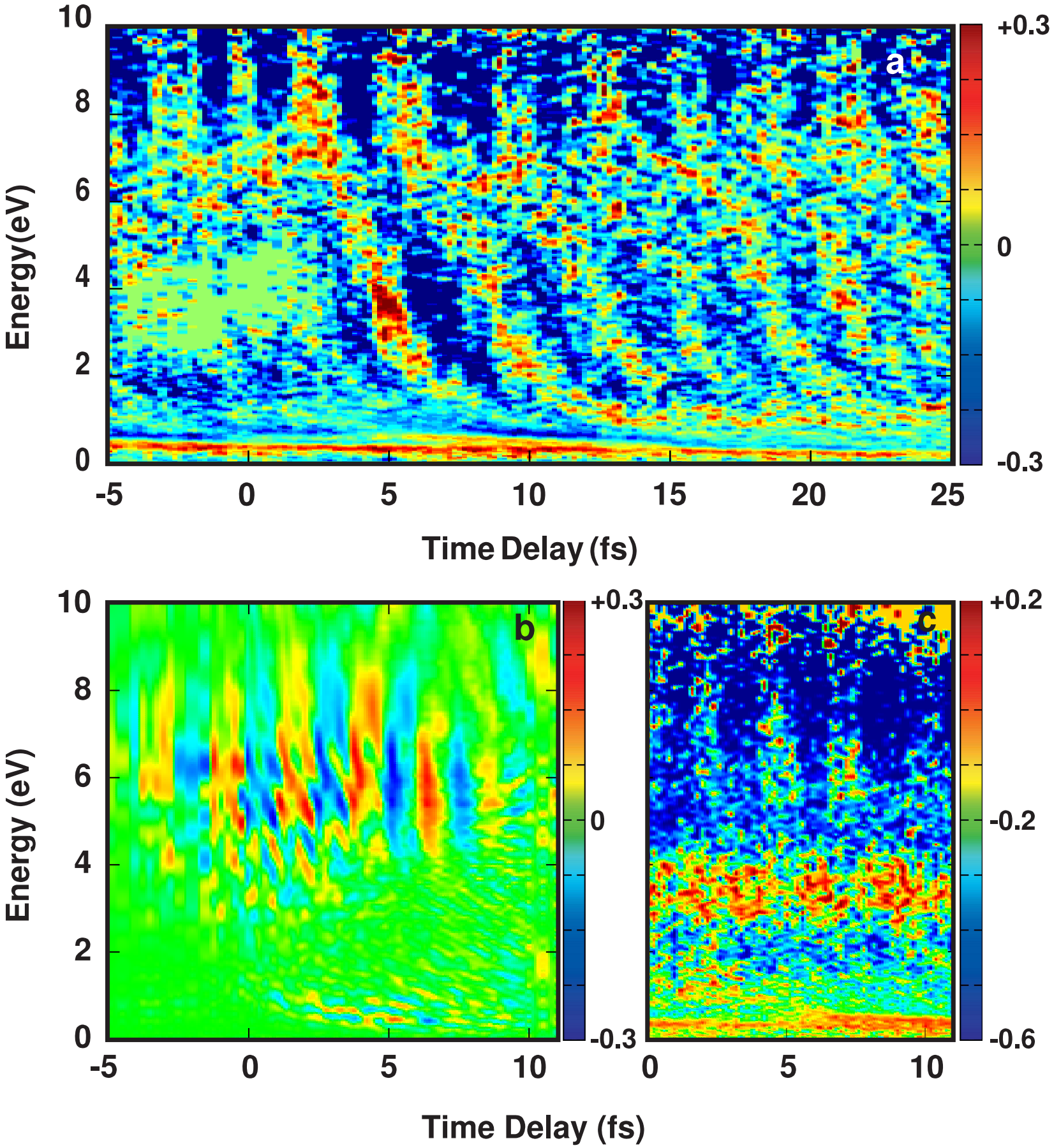
a
b
c
Energy(eV)
Energy (eV)
Time Delay (fs)
Time Delay (fs)
10
8
6
4
2
0
-5
0
5
10
15
20
25
+0.3
0
-0.3
+0.2
-0.2
-0.6

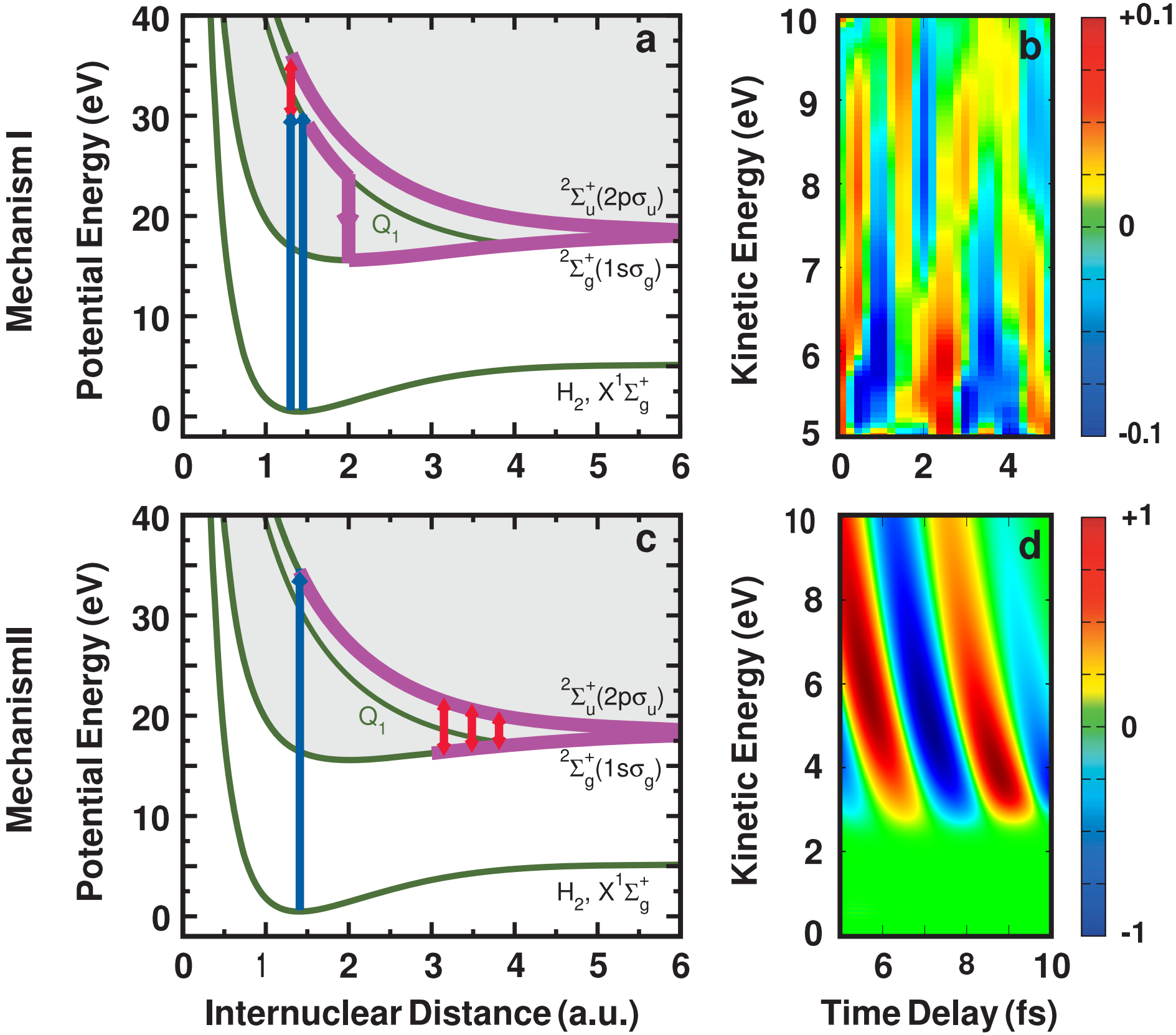
Mechanism I
Mechanism II
a
b
c
d
Potential Energy (eV)
Kinetic Energy (eV)
Internuclear Distance (a.u.)
Time Delay (fs)
$^2\Sigma_u^+(2p\sigma_u)$
$^2\Sigma_g^+(1s\sigma_g)$
H_2, $X^1\Sigma_g^+$
Q_1
+0.1
0
-0.1
+1
0
-1